Pulse compression to subcycle field waveforms with split-dispersion cascaded hollow fibers

A. A. Voronin,[1,2] J. M. Mikhailova,[2,3,4] M. Gorjan,[3,5] Zs. Major,[3,5] and A. M. Zheltikov[1,2,6,*]

[1]*Physics Department, International Laser Center, M. V. Lomonosov Moscow State University, Vorob'evy gory, Moscow 119992, Russia*

[2]*Russian Quantum Center, Skolkovo, Moscow Region 143025, Russia*

[3]*Max-Planck-Institut für Quantenoptik, Hans-Kopfermann-Strasse 1, D-85748 Garching, Germany*

[4]*A. M. Prokhorov General Physics Institute, Russian Academy of Sciences, ul. Vavilova 38, Moscow 117942, Russia*

[5]*Department für Physik, Ludwig-Maximilians-Universität München, Am Coulombwall 1, D-85748 Garching, Germany*

[6]*Department of Physics and Astronomy, Texas A&M University, College Station, Texas 77843, USA*

**Corresponding author: zheltikov@physics.msu.ru*

Received August 16, 2013; revised September 17, 2013; accepted September 18, 2013;
posted September 19, 2013 (Doc. ID 195890); published October 22, 2013

Carefully dispersion- and nonlinearity-managed cascades of gas-filled hollow-core fibers enable, as our theoretical analysis shows, efficient pulse compression with ultrahigh compression ratios. With dispersion and nonlinearity of individual fibers in such cascades optimized toward distinctly different goal functions, millijoule picosecond laser pulses can be compressed to sub-100-GW subcycle field waveforms. © 2013 Optical Society of America

OCIS codes: (320.5520) Pulse compression; (320.7110) Ultrafast nonlinear optics.
http://dx.doi.org/10.1364/OL.38.004354

Hollow-fiber-based pulse compression [1,2] is one of the key technologies of present-day ultrafast optics, capitalizing on the earlier groundbreaking achievements in fiber-based pulse compression [3–5]. Over the past few years, these technologies have been constantly progressing toward shorter pulsewidths, higher pulse energies, broader output spectra, and more accurate control over the properties of compressed pulses [6,7]. As the most recent breakthrough, synthesis of high-energy subcycle optical pulses with an unprecedented control over field waveforms has been demonstrated [8]. Cascading of hollow fibers [9] can drastically enhance the spectral broadening and temporal compression of ultrashort laser pulses [10,11]. The key argument behind this strategy of pulse compression is based on a simplified theory of self-phase modulation (SPM), where the deviation of the instantaneous frequency of the field, $\omega(\eta)$, from its central frequency ω_0 (η is the retarded time in the frame of reference related to the pulse), $\Delta\omega(\eta) = \omega(\eta) - \omega_0$, is controlled by the time derivative of the intensity envelope $I(\eta)$ [12], $\Delta\omega(\eta) \propto \partial I(\eta)/\partial\eta$. With a standard estimate $|\partial I(\eta)/\partial\eta| \sim I_0/\tau$, where I_0 is the maximum field intensity and τ is the pulsewidth, the maximum SPM-induced bandwidth $\Delta\omega_{\mathrm{SPM}}$ scales as τ^{-2}. This strong dependence of $\Delta\omega_{\mathrm{SPM}}$ on τ suggests that a pulse compression stage between two hollow fibers of equal length L can enhance spectral broadening relative to a single hollow fiber of length $2L$.

Here, we show by means of numerical simulations that, alongside the strong dependence of SPM-induced broadening on the pulsewidth, dispersion becomes a central factor for the performance of hollow-fiber-cascade pulse compressors when laser pulses acquire bandwidths supporting compression to single-cycle pulsewidths. In the following, we identify distinctly different optimization strategies for individual stages of cascaded hollow-fiber pulse compressors. While standard hollow-fiber compressors typically compress sub-50-fs pulses to few- or single-cycle pulsewidths, cascades of hollow fibers (Fig. 1) with carefully optimized dispersion and nonlinearity will be shown to allow millijoule picosecond laser pulses to be compressed to high-contrast sub-100-GW subcycle field waveforms. This latter option is of special value for rapidly progressing thin-disk laser sources, delivering high output powers at multikilohertz and megahertz repetition rates [13,14].

The model used in this work to simulate the propagation dynamics of high-energy near-IR laser pulses in cascades of gas-filled hollow fibers is based on an appropriate modification of the generalized nonlinear Schrödinger equation (GNSE) [15–17], which includes dispersion effects, Kerr nonlinearity of the gas filling the hollow fiber, ionization-induced loss and nonlinearity, shock-wave effects, as well as the leakage of modes from the hollow fiber:

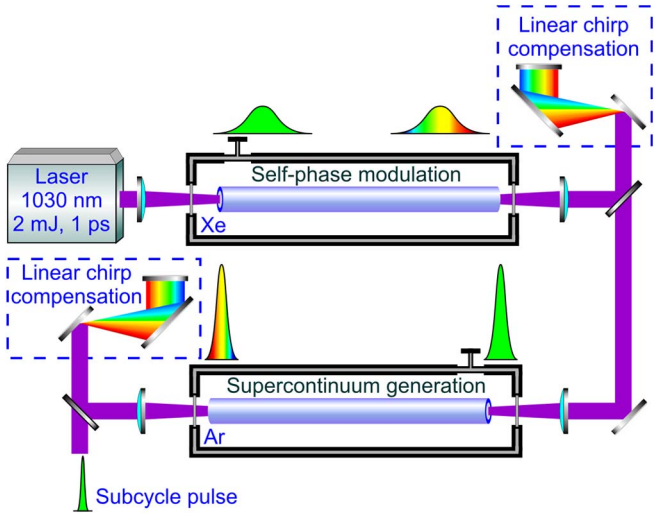

Fig. 1. Pulse compression with cascaded gas-filled hollow fibers.

$$\frac{\partial}{\partial z}A(\omega,z) = [i\hat{D}(\omega) - \alpha(\omega)]A(\omega,z) + \hat{F}\left[i\frac{n_2}{c}\omega_0\hat{T}|A(\eta,z)|^2A(\eta,z) - \frac{i\omega_0}{2n_0c\rho_c\hat{T}}\rho A(\eta,z) - \frac{(\rho_0-\rho)U_iW}{2|A(\eta,z)|^2}A(\eta,z) - \frac{\sigma(\omega_0)}{2}\rho A(\eta,z)\right].$$

Here, $A(\eta,z)$ is the complex field amplitude, $A(\omega,z)$ is its Fourier transform, η is the retarded time, ω is the frequency, z is the propagation coordinate, $D = \beta(\omega) - \beta(\omega_0) - \partial\beta/\partial\omega|_{\omega o}(\omega-\omega_0)$ is the dispersion operator, ω_0 is the central frequency of the input laser field, $\beta(\omega)$ is the propagation constant of the relevant waveguide mode, $\alpha(\omega)$ is the linear loss due to hollow-fiber mode leakage, $\hat{F}$ is the Fourier transform operator, n_2 is the nonlinear refractive index, c is the speed of light in vacuum, $\hat{T} = 1 + i\omega_0^{-1}\partial/\partial\eta$, n_0 is the refractive index at the frequency ω_0, ρ is the electron density, W is the photoionization rate, $U_i = U_0 + U_{\rm osc}$, U_0 is the ionization potential, $U_{\rm osc} = e^2I/(2\varepsilon_0cm e\omega^2)$ [15] is the energy of field-induced electron oscillations, $\rho_c = \omega_0m_e\varepsilon_0/e^2$ is the critical plasma density, m_e and e are the electron mass and charge, respectively, ρ_0 is the initial density of neutral species, $\sigma(\omega) = e^2\tau_c[m_e\varepsilon_0c(1+\omega^2\tau^2)]^{-1}$ is the inverse bremsstrahlung cross section, and τ_c is the electron collision time [16].

In our model, the GNSE is solved jointly with the equation for electron-density dynamics, including photoionization and impact ionization. The photoionization rate was calculated using the Keldysh formalism [18]. Impact ionization was modeled using the Drude-model formula for the bremsstrahlung cross section [15]. The gas dispersion is included in the model using the Sellmeier-formula coefficients from [19]. Parameters of the gas and the waveguide are chosen in such a way [20,21] as to avoid laser-induced damage of the waveguide and to keep the electron density inside the fiber core seven to 11 orders of magnitude lower than the critical electron density.

The input laser pulses were assumed to have a Gaussian temporal envelope with an FWHM pulsewidth $\tau_0 = 1$ ps, a central wavelength $\lambda_0 = 1030$ nm, and an energy $E_0 = 1.4$ mJ. The spectrum of input laser pulses is shown by the dashed line in Fig. 2. Parameters of the input laser pulses are chosen in such a way as to mimic a typical amplified thin-disk laser output [13,14]. Pulse compression within this range of parameters is known to be a challenging problem because of the long pulsewidth and high energy of input laser pulses. We show below that this problem can be solved with the use of properly dispersion- and nonlinearity-optimized cascades of gas-filled hollow-core fibers.

To this end, we consider a cascade of two hollow fibers (Fig. 1), where SPM-induced spectral broadening in the first fiber of the cascade is followed by pulse compression, providing the input for the second hollow fiber of the cascade. Dispersion and nonlinearity optimization strategies for the two fibers in the cascade are drastically

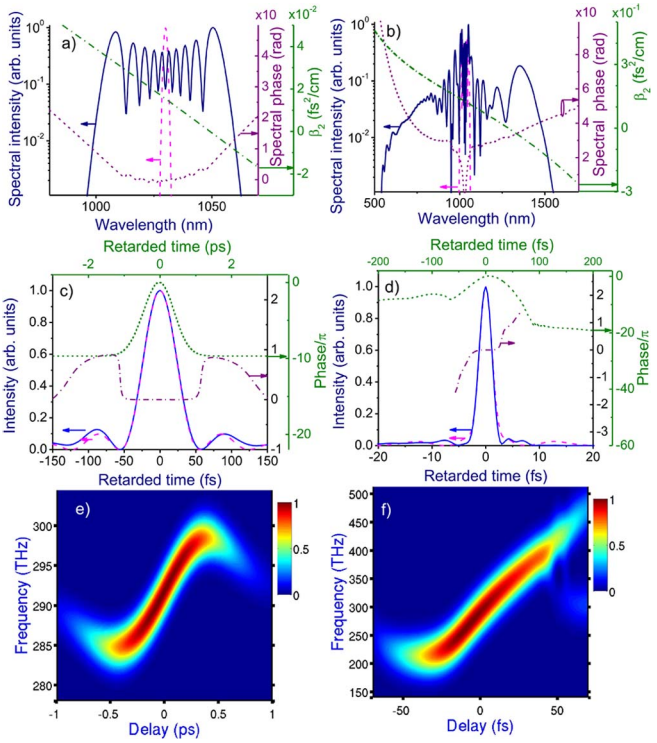

Fig. 2. Pulse compression with a cascade of two gas-filled hollow fibers consisting of a first fiber with $d = 285$ μm and $L = 200$ cm filled with xenon at $p = 1$ bar and a second fiber with $d = 360$ μm and $L = 300$ cm filled with argon at $p = 1.35$ bar: (a), (b) spectra at the input (dashed line) and output (solid line) of (a) first and (b) second fiber with a dispersion profile as shown by the dashed–dotted lines. The output spectral phase is shown by the dotted line. (c), (d) Envelope (solid line) and phase (dashed–dotted line) of the output of (c) first and (d) second fiber compressed through a compensation of the linear chirp only, the phase of the fiber output (dotted line, upper time scale), and the transform-limited pulse supported by the entire spectrum at the output of the nonlinear medium (dashed line). (e), (f) Spectrograms for the pulses at the output of (e) first and (f) second fibers.

different because of dramatically different pulsewidths and bandwidths of field waveforms at the input of these fibers. The first fiber, intended to provide efficient spectral broadening of long, 1 ps laser pulses, is designed in such a way as to achieve an acceptable compromise between the efficiency of SPM, which dictates small fiber inner diameters d, and the waveguide loss combined with the risk of laser damage of the fiber walls, both rapidly growing with a decrease in d.

This assignment is fulfilled with a hollow fiber with an inner diameter $d = 285$ μm filled with xenon at a pressure $p = 1$ atm. The fiber length, $L = 200$ cm, is chosen in such a way as to maximize SPM-induced spectral broadening in a fiber with a loss [12]. With such a choice of parameters, the energy fluence on the fiber walls is at least two times lower than the laser-damage threshold ($\approx$2 J/cm^2 [22,23]), while the waveguide loss of 38%, corresponding to a throughput of 62%, is still acceptable. The utility of few-meter-long gas-filled hollow fibers for the spectral broadening of ultrashort laser pulses has been demonstrated by Nagy *et al.* [24]. Xenon is chosen due to its high nonlinearity. The ionization potential for

xenon is $U_0 = 12.06$ eV, $\tau_c = 190(p_{\text{atm}}/p)$ fs [15], and the nonlinear refractive index is $n_2 = 8 \cdot 10^{-19}$ (p/p_{atm}) cm^2 W^{-1}, p_{atm} being the atmospheric pressure [25]. The input peak power of laser pulses for this set of parameters, $P \approx 1.3$ GW, is approximately a factor of 1.5 lower than the critical power of self-focusing for a freely propagating beam, $P_{\text{cr}} = 3.72\lambda^2/(8\pi n_0 n_2)$, where n_0 is the refractive index, giving $P_{\text{cr}} \approx 2$ GW for Xe at $p \approx 1$ atm and $\lambda = 1030$ nm.

SPM, which dominates the nonlinear evolution of laser pulses in the first fiber, gives rise to a trademark symmetric broadening of their spectra [Fig. 2(a)]. The spectral bandwidth at the fiber output is quite accurately described in this regime by a standard estimate [12] $\varepsilon \approx \varepsilon_0 = (1 + (0.88 \cdot B)^2)^{1/2}$, where $\varepsilon = \Delta\omega_{\text{out}}/\Delta\omega_{\text{in}}$, $\Delta\omega_{\text{in}}$, and $\Delta\omega_{\text{out}}$ are the input and output bandwidths, and B is the B integral. In the regime of spectral broadening illustrated in Fig. 2(a), our numerical simulations give $\varepsilon \approx 26.8$ and $B \approx 30.8$. The ε_0 ratio calculated with such a B is only 1% larger, $\varepsilon_0 \approx 27.1$.

Following linear chirp compensation (LCC), e.g., using a grating pulse compressor, whose throughput is taken equal to 75%, the fiber output is transformed into a pulse with the FWHM pulsewidth of the central peak $\tau \approx 51.7$ fs. The transform-limited pulsewidth supported by the entire spectrum of the fiber output is $\tau_l \approx$ 51.2 fs [dashed line in Fig. 2(c)], which is only 0.5 fs shorter than the LCC pulsewidth, indicating efficient suppression of high-order phase distortions [dashed–dotted line in Fig. 2(c)].

To quantify the quality of pulse compression, we use the ratio $Q = E_p/E_t$ of the energy E_p contained within 3τ in the central peak of the compressed pulse to the total energy of the output pulse E_t. A small Q means that a pulse contains a powerful pedestal, while Q close to unity corresponds to a high-contrast pulse. For the 51.7 fs compressed pulse behind the first stage of the fiber cascade, $Q_1 = E_{p1}/E_{t1} \approx 63\%$ [solid line in Fig. 2(c)], where E_{p1} is the energy of the central peak in the compressed output and E_{t1} is the total energy of the compressed pulse.

We now let the LCC-compressed output of the first fiber propagate through the second hollow-filled waveguide in our cascade. Since the pulses are much shorter at this stage of pulse compression, with their SPM-broadened spectra spanning over more than an octave toward the output end of the fiber [Fig. 2(b)], self-steepening starts to contribute to the nonlinear dynamics, enhancing the high-frequency part of the spectrum and making the phase profile of the field more complicated [dotted line in Fig. 2(d) and the map of Fig. 2(f)]. The phase of the field becomes even more distorted when the long-wavelength part of the spectrum falls beyond the zero-GVD point into the range of anomalous dispersion [Fig. 2(b)]. In view of these effects, a drastically different strategy of fiber optimization is needed at this stage to include conflicting requirements on pulse parameters imposed by the efficiency of spectral broadening and pulse compression quality.

As the inner diameter of the second fiber is set equal to its minimum value, $d = 240$ μm, corresponding to a laser damage of fiber walls (shown by the dashed vertical line in Fig. 3), pulses as short as 2.0 fs can be generated

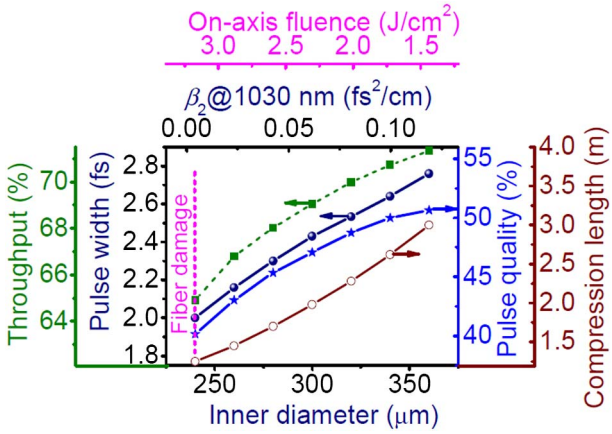

Fig. 3. Optimization scan for the second fiber in the cascade for an input laser pulse with a spectrum and temporal envelope as shown in Figs. 2(a) and 2(c): the LCC-compressed pulsewidth (filled circles), throughput (rectangles), pulse compression quality (asterisks), and optimal compression length (open circles) are shown as ordinate axes; the inner fiber diameter, the second-order fiber dispersion coefficient, and the on-axis fluence are given along the abscissa axis. The boundary of the fiber laser-damage threshold is shown by the vertical dashed line.

through an LCC of the output of an a 1.25 m stretch of hollow fiber filled with argon ($n_2 = 1.15 \cdot 10^{-19}$ (p/p_{atm}) cm^2 W^{-1} [25], $U_0 = 15.76$ eV, and $\tau_c = 190$ (p_{atm}/p) fs [14]) at $p = 1.35$ bar (Figs. 3 and 4). The peak power of laser pulses at the input of the second fiber, $P \approx 6.8$ GW, is approximately a factor of 1.5 lower than the critical power of self-focusing for a freely propagating beam, $P_{\text{cr}} \approx 10$ GW for Ar at $p \approx 1.35$ atm and $\lambda =$ 1030 nm. The electron density on the axis of the hollow fiber in this regime was on the order of 10^{14} cm^{-3}, still having virtually no influence on field dynamics. A moderate pulse compression quality in this regime, $Q_2 = E_{p2}/E_{t2} \approx 40\%$ (asterisks in Fig. 3), reflects severe phase

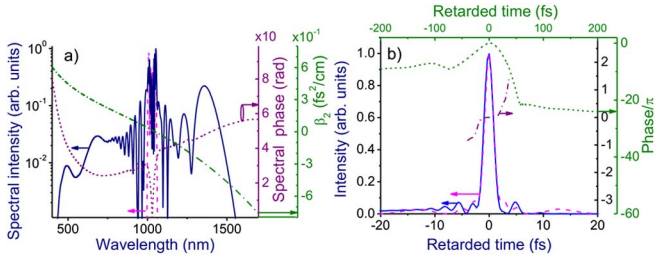

Fig. 4. Pulse compression with a cascade of two gas-filled hollow fibers consisting of a first fiber with $d = 285$ μm and $L =$ 200 cm filled with xenon at $p = 1$ bar and a second fiber with $d = 240$ μm and $L = 125$ cm filled with argon at $p = 1.35$ bar: (a) spectra at the input (dashed line) and output (solid line) of the second fiber with a dispersion profile as shown by the dashed–dotted line; the output spectral phase is shown by the dotted line. (b) Envelope (solid line) and phase (dashed–dotted line) of the output of the second fiber compressed through a compensation of the linear chirp only, the phase of the fiber output (dotted line, upper time scale), and the transform-limited pulse supported by the entire spectrum at the output of the nonlinear medium (dashed line).

distortions [Figs. 4(a) and 4(b)] arising when the red wing of the spectrum falls beyond the zero-GVD wavelength $\lambda_z \approx 1050$ nm [Fig. 4(a)]. With larger fiber inner diameters, the zero-GVD wavelength is shifted to longer wavelengths [$\lambda_z \approx 1300$ nm for $d = 360$ μm; Figs. 2(b) and 3], allowing slightly longer but still subcycle pulses to be generated [Figs. 2(d) and 3] with a substantially higher compression quality and a higher throughput (rectangles and asterisks in Fig. 3). The on-axis electron density in this regime never exceeded 10^{11} cm^{-3}, leading to no detectable changes in field dynamics.

In Figs. 2(b) and 2(d), we show how an LCC-compressed output of the first fiber of the cascade [dashed line in Fig. 2(c)] can be transformed to a subcycle field waveform through spectral broadening in a hollow fiber with $d = 360$ μm and $L = 300$ cm filled with argon at $p = 1.35$ atm. Such a fiber provides normal dispersion up to a zero-GVD wavelength at 1300 nm [dashed–dotted line in Fig. 2(b)]. The supercontinuum generated at the output of such a waveguide with a throughput of 71% has a spectrum spanning over more than an octave [solid line in Fig. 2(b)], supporting a transform-limited pulse with $\tau_l \approx 2.8$ fs [dashed line in Fig. 2(d)]. Pulse compression based on LCC yields a pulse featuring the main peak with $\tau \approx 2.8$ fs [solid line in Fig. 2(d)] with a compression quality $Q_2 = E_{p2}/E_{t2} \approx 50\%$, where E_{t2} is the total energy of the compressed pulse at the output of the second fiber. The main peak of the compressed pulse carries an energy $E_{p2} \approx 0.17$ mJ, providing a peak power of about 61 GW in a subcycle field waveform.

For octave-spanning spectra achieved in the second fiber, supporting single-cycle, and even subcycle transform-limited pulsewidths, self-steepening and high-order dispersion effects start to play an important role, giving rise to asymmetric spectra [Fig. 2(b)] and complex phase profiles [Figs. 2(b) and 2(d)]. In these regimes, simple relations between the spectral broadening and the B integral fail. Indeed, while for the B integral achieved in our simulations presented in Figs. 2(b) and 2(d), $B \approx 27.7$ dictates $\varepsilon_0 \approx 24.4$, the spectral broadening observed in simulations corresponds to $\varepsilon \approx 13.4$.

The optimal fiber length L_{opt} for pulse compression in this regime of extremely short field waveforms can also drastically differ from the standard result largely based on slowly varying envelope approximation (SVEA) analysis, giving [5] $L_{\mathrm{opt}} \sim (L_d L_{\mathrm{nl}})^{1/2}$, where $L_d = \tau_0^2/|\beta_2|^{-1}$ is the dispersion length, $\beta_2 = \partial^2\beta/\partial\omega^2$ is the GVD coefficient, and $L_{\mathrm{nl}} = c/(\omega n_2 I)$ is the nonlinear length. Specifically, with the dispersion and nonlinear lengths estimated as $L_d = 76.4$ m and $L_{\mathrm{nl}} = 7.6$ cm using the input pulsewidth for the second fiber in our pulse compressor, the SVEA gives the following optimal fiber length for pulse compression: $L_{\mathrm{opt}} = 1.4(L_d L_{\mathrm{nl}})^{1/2} \approx 340$ cm. Numerical simulations, on the other hand, show that the optimal compression is achieved with a 3 m stretch of fiber.

To summarize, we have shown that cascaded hollow-core fibers with properly managed dispersion and nonlinearity can enable a high-throughput compression of millijoule picosecond laser pulses to high-contrast sub-100-GW subcycle field waveforms.

Stimulating discussions with and continuous support from F. Krausz are gratefully acknowledged. This research was supported in part by the Russian Foundation for Basic Research (Project Nos. 13-02-92115, 13-02-01465, and 13-04-40335), the Welch Foundation (Grant No. A-1801), the Skolkovo Foundation (Grant No. 78), and the Munich Center for Advanced Photonics (MAP) as a part of the DFG Excellence Initiative.

References

1. M. Nisoli, S. De Silvestri, and O. Svelto, Appl. Phys. Lett. **68**, 2793 (1996).
2. M. Nisoli, S. De Silvestri, O. Svelto, R. Szipöcs, K. Ferencz, C. Spielmann, S. Sartania, and F. Krausz, Opt. Lett. **22**, 522 (1997).
3. D. Grischkowsky and A. C. Balant, Appl. Phys. Lett. **41**, 1 (1982).
4. W. J. Tomlinson, R. H. Stolen, and C. V. Shank, J. Opt. Soc. Am. B **1**, 139 (1984).
5. J.-C. Diels and W. Rudolph, *Ultrashort Laser Pulse Phenomena* (Elsevier, 2006).
6. A. Wirth, M. T. Hassan, I. Grguraš, J. Gagnon, A. Moulet, T. T. Luu, S. Pabst, R. Santra, Z. A. Alahmed, A. M. Azzeer, V. S. Yakovlev, V. Pervak, F. Krausz, and E. Goulielmakis, Science **334**, 195 (2011).
7. A. M. Zheltikov, Phys. Usp. **45**, 687 (2002).
8. M. Hassan, A. Wirth, I. Grguras, A. Moulet, T. Luu, J. Gagnon, V. Pervak, and E. Goulielmakis, Rev. Sci. Instrum. **83**, 111301 (2012).
9. M. Nisoli, G. Sansone, S. Stagira, C. Vozzi, S. De Silvestri, and O. Svelto, Appl. Phys. B **75**, 601 (2002).
10. N. Zhavoronkov and G. Korn, Phys. Rev. Lett. **88**, 203901 (2002).
11. B. Schenkel, J. Biegert, U. Keller, C. Vozzi, M. Nisoli, G. Sansone, S. Stagira, S. De Silvestri, and O. Svelto, Opt. Lett. **28**, 1987 (2003).
12. G. P. Agrawal, *Nonlinear Fiber Optics* (Academic, 2001).
13. T. Metzger, A. Schwarz, C. Y. Teisset, D. Sutter, A. Killi, R. Kienberger, and F. Krausz, Opt. Lett. **34**, 2123 (2009).
14. S. V. Marchese, C. R. E. Baer, R. Peters, C. Kränkel, A. G. Engqvist, M. Golling, D. J. H. C. Maas, K. Petermann, T. Südmeyer, G. Huber, and U. Keller, Opt. Express **15**, 16966 (2007).
15. L. Bergé, S. Skupin, R. Nuter, J. Kasparian, and J.-P. Wolf, Rep. Prog. Phys. **70**, 1633 (2007).
16. A. Couairon and A. Mysyrowicz, Phys. Rep. **441**, 47 (2007).
17. A. M. Zheltikov, A. A. Voronin, R. Kienberger, F. Krausz, and G. Korn, Phys. Rev. Lett. **105**, 103901 (2010).
18. L. V. Keldysh, Zh. Eksp. Teor. Fiz. **47**, 1945 (1964).
19. M. J. Weber, *Handbook of Optical Materials* (CRC Press, 2003).
20. A. A. Voronin, V. M. Gordienko, V. T. Platonenko, V. Ya. Panchenko, and A. M. Zheltikov, Opt. Lett. **35**, 3640 (2010).
21. G. Andriukaitis, D. Kartashov, D. Lorenc, A. Pugžlys, A. Baltuška, L. Giniūnas, R. Danielius, J. Limpert, T. Clausnitzer, E.-B. Kley, A. Voronin, and A. Zheltikov, Opt. Lett. **36**, 1914 (2011).
22. X. Chen, A. Jullien, A. Malvache, L. Canova, A. Borot, A. Trisorio, C. G. Durfee, and R. Lopez-Martens, Opt. Lett. **34**, 1588 (2009).
23. S. Bohman, A. Suda, T. Kanai, S. Yamaguchi, and K. Midorikawa, Opt. Lett. **35**, 1887 (2010).
24. T. Nagy, V. Pervak, and P. Simon, Opt. Lett. **36**, 4422 (2011).
25. H. J. Lehmeier, W. Leupacher, and A. Penzkofer, Opt. Commun. **56**, 67 (1985).